Molecular Simulation of Folding and Aggregation of Multi-Core Polycyclic Aromatic Compounds

Xiaoyu Sun[a], *Hongbo Zeng*[a,*], *Tian Tang*[b,*]

[a]*Department of Chemical and Materials Engineering, University of Alberta, Edmonton, AB T6G 1H9, Canada*

[b]*Department of Mechanical Engineering, University of Alberta, Edmonton, AB T6G 1H9, Canada*

** Corresponding authors*

E-mail addresses: xsun4@ualberta.ca (X. Sun); hongbo.zeng@ualberta.ca (H. Zeng); tian.tang@ualberta.ca (T. Tang).

Phone: +1-780-492-1044 (H. Zeng); +1-780-492-5467 (T. Tang).

Fax: +1-(780)-492-2881 (H. Zeng); +1-780-492-2378 (T. Tang).

Declarations of interest: none

Abstract

Compared with polycyclic aromatic compounds (PACs) that have a single polyaromatic core, those having multiple cores connected by aliphatic chains can undergo significant internal conformational change, leading to folding, the stacking between the cores within the same molecule. In this work, we investigated this interesting phenomenon using molecular dynamics simulations, performed in three different solvents: water, heptane and toluene. In addition, by having several multi-core PACs in the same solution, the relationship between intramolecular folding and intermolecular aggregation was elucidated. In water, a single multi-core PAC preferred to stay in the unfolded state; contrarily, folded configuration became dominant when multiple molecules aggregated. In heptane and toluene, a multi-core PAC molecule could switch easily between folded and unfolded configurations, regardless of whether it was in single dispersed or aggregated states. Introduction of single-core PACs further modified the folding characteristics of multi-core PACs in water and heptane. This work provided fundamental insights into the interplay between folding, homoaggregation (between multi-core PACs) and heteroaggregation (between multi-core and single-core PACs) in a colloidal system.

Keywords

Folding; Aggregation; Polycyclic aromatic compound; Molecular dynamics simulation.

1. Introduction

Flexible molecules in colloidal systems undergo dynamic motion and conformational changes driven by many non-covalent interactions, such as hydrogen bonding, van der Waals forces, π-π interactions, electrostatic interactions, etc. Internally, different parts of the same molecule can interact forming interesting configurations [1]. One such example is the folding of biomacromolecules such as protein [2–4]. Molecular folding has also been studied in many other applications, including biomedical [5,6], environmental [7,8], food science [9,10], and chemical engineering [11,12]. On the other hand, interactions among different molecules can lead to aggregation and even assembly of ordered structures in colloidal systems, which has found applications in a number of areas [13,14]. In this work we investigate a class of interesting molecules, polycyclic aromatic compounds (PACs), which are susceptible to both intramolecular conformational changes and intermolecular aggregation.

PAC has two subgroups: polycyclic aromatic hydrocarbon which has two or more fused benzene rings with only carbon and hydrogen atoms, and heterocyclic aromatic hydrocarbons which contain heteroatoms [15,16]. A large fraction of PACs exist naturally in coal, oil, wood, tar, etc. [17], while some have been synthesized for nanotechnology applications [18–21]. It is known that PACs tend to stack through intermolecular π−π interactions between their polyaromatic (PA) cores [22,23]. In fact, self-assembly of PACs into columnar superstructures has led to intriguing nanostructures [24–26] that can function as optical and electronic devices [27–30]. The PA cores in a PAC can have different sizes and structures, such as acenaphthene, fluoranthene, pyrene, etc. [15,24] In addition, a PAC can contain one large PA core, or multiple small cores connected by aliphatic linkers. For example, structures of asphaltenes, a component of crude oil, are typically categorized as continental type (single-core) and archipelago type (multi-core). Adamson et al.

[31], using tandem mass spectrometry, detected aliphatically-bridged multi-core PACs in sooting flames. Alvariño et al. [25] synthesized metallacycles of PACs with multiple aromatic regions and matched the dimension of cavity to dinuclear receptors, which was of interest for applications such as drug delivery. Pisula et al. [22] studied columnar assembly of disk-like PA cores in electronic applications; by attaching side chains with or without other PA cores, the mobility of charge carrier could be tuned. Mativetsky et al. [32] synthesized self-assembled monolayer of multi-core bridged PACs that could be applied as a new donor-acceptor dyad. While the intermolecular aggregation or self-assembly have been frequently studied for single-core PACs [33–36], much less attention has been paid to multi-core PACs [22,25,31,32]. Furthermore, compared with single-core PACs, multi-core PACs are usually more flexible and susceptible to internal structural changes. This has motived the present study, where we investigate both aggregation and folding, the stacking between the cores within the same molecule, of multi-core PACs.

Studies on the colloidal behaviours of multi-core PACs have been limited. Acevedo et al. [37] calculated the solubility parameter of PACs in 57 organic solvents, and found multi-core PACs to be more difficult to aggregate than single-core PACs [37]. To explain, the authors hypothesized that multi-core PACs may have folding and unfolding features due to their rotational degree of freedom at the interconnection between the cores, although no direct evidence was provided [37]. Kuznicki et al. [38] performed molecular dynamics (MD) simulations on a mixture of both single-core and multi-core PACs, dispersed in water, toluene and heptane. The observation of “self-stacking” was reported for multi-core PACs, similar to the folding proposed by Acevedo et al. [37] Recently, an interesting work by Wang et al. studied the aggregation and folding of multi-core PACs in toluene, n-heptane and their mixtures, using coarse-grained MD simulation and nonlinear machine learning [39]. Folding of these PACs was demonstrated to depend on the molecular structure, for example, extended (unfolded) configuration was energetically favorable for a model with two linearly connected PA cores and a model with three mutually connected PA cores, whereas a model that contained three linearly connected PA cores showed a complex free energy landscape that was concentration dependent [39]. Although different concentrations were simulated, mechanistically how the folding of individual molecules was impacted by aggregation was not addressed.

Based on the state of the literature, the present work investigated the folding of multi-core PACs and for the first time, addressed the relationship between folding and aggregation. Three commonly used solvents were applied: water (polar), heptane (aliphatic) and toluene (aromatic), to examine the potential effect of solvent. In addition, single-core PACs were introduced to study the impact of heteroaggregation on the folding of multi-core PACs. Our work contributed to the fundamental understanding of molecules in a colloidal system which are simultaneously susceptible to intramolecular conformational changes and intermolecular aggregation. The results illustrated the connections between the intra- and intermolecular behaviors, as well as the impact of surrounding environment (i.e., solvent), which may provide insights into the investigation of other complex colloidal systems.

2. Method

2.1 Models and systems

Two molecular models were constructed to represent multi-core and single-core PACs, respectively, and their chemical structures are shown in Fig. 1. The multi-core PAC is a hypothetical model that contains three aromatic cores connected by short aliphatic chains (Fig. 1a), which will be hereafter referred to as model “M”. The initial structure of model M was drawn in ChemDraw Prime 16.0. The geometry of the entire molecule was optimized using Gaussian16 [40] at B3LYP/3-31G + (d,p) level [41], and then submitted to Automated Topology Builder (ATB) [42,43] to produce the topology compatible with the GROMOS96 [44–46] united-atom force field. The partial atomic charges were calculated using Gaussian16 at B3LYP/6-31G + (d,p) level with CHELPG (CHarges from ELectrostatic Potentials using a Grid based method) [47–50], and manually assigned to the topology generated from ATB [8,51,52]. This procedure of developing the force field parameters is well-established and used extensively in the literature [41–43,47–50]. The creation of model M originated from a chemical structure proposed by Nexen Energy ULC to represent pentane-insoluble asphaltenes [53,54] in Athabasca bitumen. MD simulations were performed to calculate the density of M molecules in solid state and size of their aggregates in organic solvents, which compared well with experimental study of asphaltene samples (see Supporting Information (SI) Section SI1 for details). However, it should be emphasized that it is not the purpose of the present work to determine the quality of model M in representing asphaltenes, which is still highly debated. Rather, our focus is to investigate its folding and the interplay between folding and aggregation. The single-core PAC (Fig. 1b) is based on the compound Violanthrone-79 (VO-79), and will be hereafter referred to as model "S". This model has been simulated in the past and its force field parameters were directly adopted [65,66].

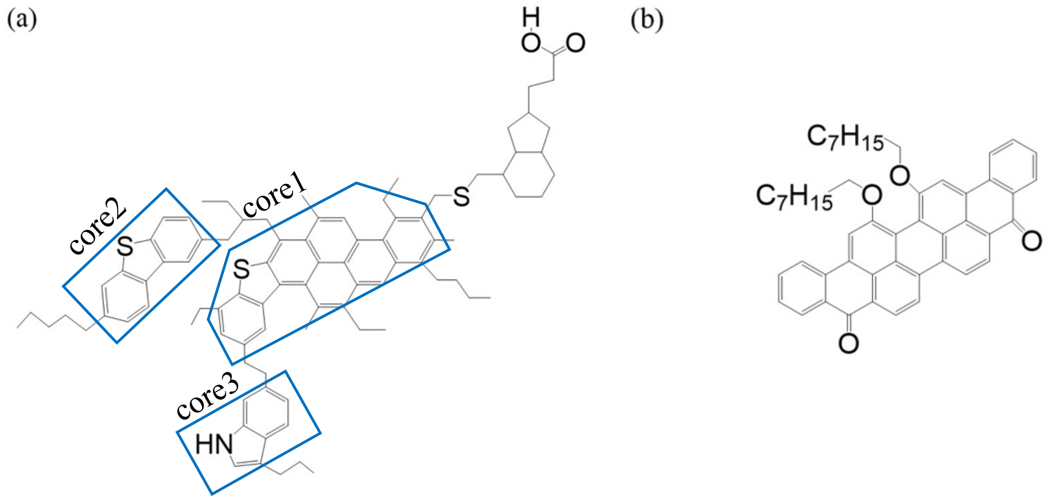

Figure 1. Molecular structure of (a) model M; and (b) model S.

Three types of solvents were selected to study folding and aggregation of PACs in colloidal systems. The first is water since PACs are common water contaminants and their behaviors in aqueous solution are of wide interest [55–57]. The other two are organic solvents, respectively aliphatic (heptane) and aromatic (toluene) in nature. They were chosen because like most of the PACs, the models in Fig. 1 contain both aromatic and aliphatic units. In fact, heptane and toluene have both been extensively used as solvents for PACs [58–64]. SPC model was used for water, while force field parameters for heptane and toluene were adopted from previous publications of Lan et al. [65,66] from our group.

A single model M molecule was solvated in water, heptane and toluene respectively, which formed systems 1, 2 and 3 as shown in Table 1. Solutions containing multiple M molecules were simulated as systems 4, 5 and 6 respectively in water, heptane and toluene. A mixture of M and S molecules were also simulated in water, heptane and toluene (systems 7, 8 and 9).

Table 1. Details of simulated systems

sys.	# of M	# of S	solvent	# of solvent molecules	initial box length (nm)
1	1	0	water	7039	6
2	1	0	heptane	1063	6
3	1	0	toluene	1132	6
4	12	0	water	56786	12
5	12	0	heptane	8450	12
6	12	0	toluene	9920	12
7	6	18	water	56542	12
8	6	18	heptane	8500	12
9	6	18	toluene	9793	12

2.2 Simulation details

All simulations were performed using GROMACS package [46,67–69] (version 5.0.7) with GROMOS 96 force field 53A6 parameter sets [70]. Each system first underwent a static structure optimization via energy minimization. Then, NVT simulation was carried out for 100 ps where non-hydrogen atoms of the model PAC molecules were restrained by a harmonic potential with constant 1000 kJ/(mol·nm^2). The restraint was removed and full dynamics simulation was carried out in NPT ensemble at 300 K and 1 bar. The pressure was controlled by Parrinello-Rahman barostat and the temperature was controlled by velocity rescaling thermostat. LINCS algorithm and Particle Mesh Ewald method for full electrostatics [71] were applied. The cut-off for non-bonded (van der Waals and electrostatic) interactions was set to 1.4 nm. Periodic boundary conditions were applied in all directions. All simulations had a time step of 2 fs and simulation time of 60 ns.

3. Results and discussion

3.1 Folding of a single M molecule

Systems 1 to 3 examine the conformation changes of a single M molecule in the three solvents. From the root-mean-square deviation (RMSD) of the molecule (SI Section SI2), in the last 50 ns, configuration of the single M molecule became relatively stable in water, while the molecule in heptane or toluene underwent more dynamic but reversible conformational changes. Data in the last 50 ns representing dynamic equilibrium were analyzed. Because the interconnecting chains in the M molecule allow for internal degree of freedom, it was observed that sometimes during the simulation trajectory, two aromatic cores within the molecule could approach each other and exhibit stacking or parallel alignment. An example for such a configuration is shown in Fig. 2a and 2b. The aromatic cores may also stay un-stacked, as shown in Fig. 2c and 2d. Dynamic conversion between the two types of configurations, i.e., folding and unfolding of the molecule, was observed.

In order to quantify folding and unfolding, the distance (D) between the centers of geometry (COGs) of core1 and core2 (see Figure 1a for definition) was calculated, along with the angle (θ) between the two cores. As shown in Fig. 1a, core1 contains 6 aromatic rings, core2 contains 2 aromatic rings, whereas core3 only has one aromatic ring. It is therefore expected that among the three cores, the interaction between core1 and core2 is the strongest and plays dominant role in folding. This was confirmed by the generally larger distance between core3 and core1 than that between core2 and core1 (see SI, Section SI3 for details). To calculate D and θ, each core was approximated by a plane defined by three atoms, two carbon atoms shown in cyan and one sulfur shown in yellow in Fig. 2. The COG of these three atoms was calculated to represent the COG of each core. θ was calculated as the angle between the positive normal of the two planes. Therefore, when θ is close to 0 or 180° the two cores are nearly parallel to each other (see SI, Section SI4 for more details). In Fig. 2c-d, D = 1.0 nm and θ = 137°, whereas in Fig. 2a-b, D = 0.4 nm and θ =

173°. The reduction in separation along with θ approaching 180° is an indication of stacking between the two cores, i.e., folding of the molecule.

(a) Folded configuration (top view) (c) Unfolded configuration (top view)

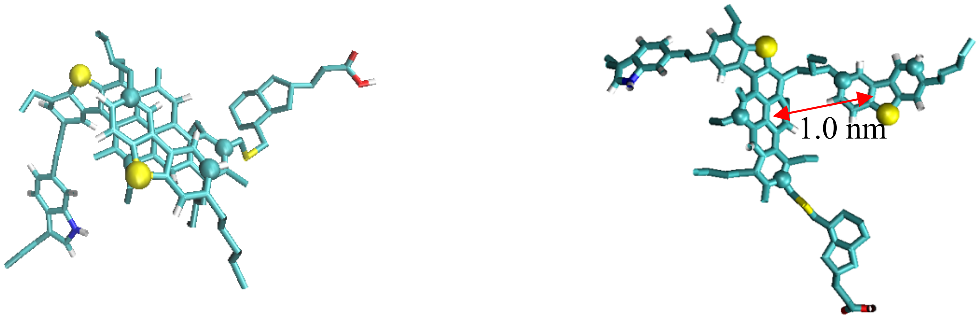

(b) Folded configuration (side view) (d) Unfolded configuration (side view)

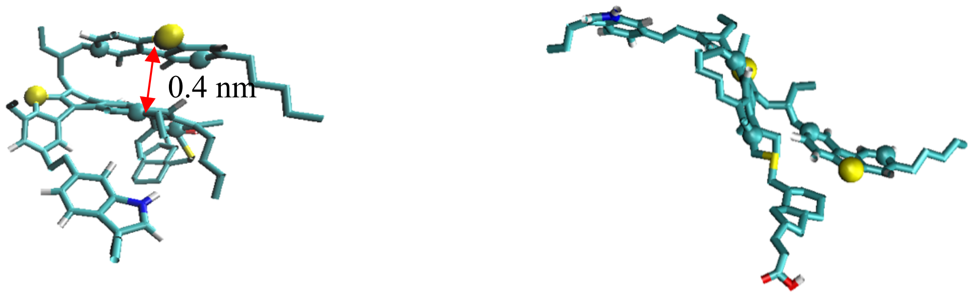

Figure 2. Left panel: a representative folded configuration of the M molecule in toluene (a) top view, (b) side view. Right panel: a representative unfolded configuration for the same molecule (c) top view, (d) side view. Distance between core1 and core2 are indicated in (b) and (c), and three atoms defining the plane of each core are highlighted in each subfigure.

D and θ values were collected along the simulation trajectory for the last 50 ns (one data every 10 ps, 5000 data points in total) and plotted against each other in Fig. 3. For *D*, the data naturally separates into groups that are either slightly smaller than 0.55 nm, or greater than 0.55 nm. For θ, separation of data can be observed at around 140°. As stated earlier, angles close to 180° or 0° represent nearly parallel stacking of core1 and core2. Considering symmetry, in this work the molecule will be defined to be in a folded state when $D \leq 0.55$ nm and θ is either <40° or >140°. If $D \leq 0.55$ nm but θ is between 40° and 140°, the two cores have close contact but are not parallel, and we describe the molecule as being in a partially folded state. The molecule is in an unfolded state if $D > 0.55$ nm. Further explanation on using 0.55 nm as the criterion is given in Supporting Information Section SI5.

In water, Fig. 3a shows two distinct bands for the collected data (highlighted by black lines): one with D slightly below 0.75 nm and θ in the range of 20° to 100°, representing the unfolded state; and the other with D slightly below 0.55 nm and θ in the range of 140° to 180°, representing the folded state. There is a clear gap between $\theta = 100°$ and $\theta = 140°$ where few data points exist, suggesting an energy barrier for the transition between folded and unfolded states. Additional evidence for this barrier is shown in SI (Section SI6) where the molecule stayed in the unfolded state for the first 56 ns, then became folded and stayed in such state for the rest of the simulation. The folded configuration is favored by the π–π interaction between the hydrophobic PA cores, while the unfolded configuration is favored by the release of stress in the linkers connecting the cores as well as the entropy gain from the dissociation of cores. Dynamic motion of the small water molecules also tends to destabilize the folded configuration of a single molecule. Consequently, the M molecule spends the majority of the time in the unfolded state.

In heptane, as shown in Fig. 3b, a band near $\theta = 180°$ (highlighted by black line) can be recognized as the molecule being in the folded state. This band is continuous with another band (highlighted by another black line) where D =~0.55 nm and θ is between 50° and 140°, corresponding to partially folded state. There are also considerable amounts of data for the folded state near $\theta = 0°$. Compared with water, data corresponding to the unfolded state do not form a narrow band. Instead, there is a cloud-like distribution spanning a large range of D (from 0.55 nm to 1 nm). The molecule shows much more flexibility in heptane, which can also be seen from the larger fluctuations in θ (SI, Section SI6) along the simulation trajectory. Data in toluene (Fig. 3c) exhibit similar features as in heptane, except that partial folding of the molecule is almost absent. The lack of partial folding could be caused by the interaction between the aromatic cores of toluene and PA cores on the M molecule, which tends to destabilize a partially folded configuration.

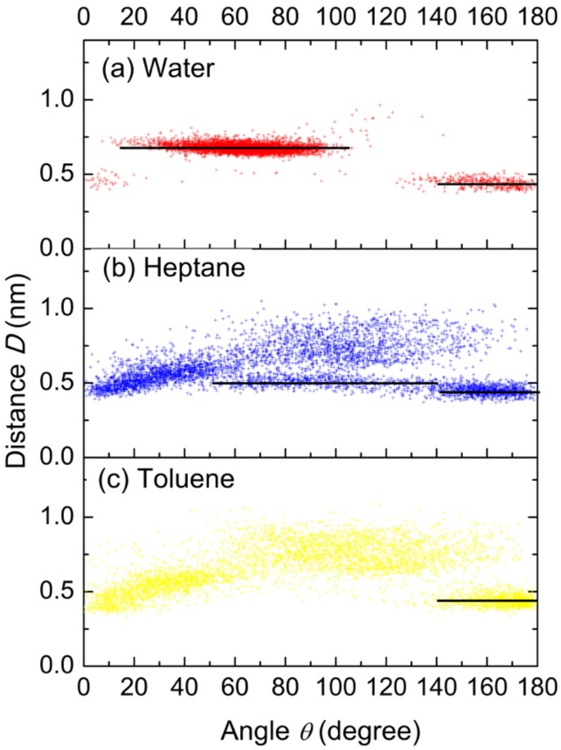

Figure 3. Distance D between COGs of core1 and core2 versus angle θ between the two cores. Data are from simulations of a single M molecule in (a) water, (b) heptane and (c) toluene.

Based on the criteria introduced above, the numbers of folded, unfolded and partially folded states were counted from the 5000 frames in the last 50 ns of the simulations, from which the probability of each state was calculated, as shown in Table 2. The free energy change from state 1 to state 2 was then be estimated from [72]:

$$\Delta G = G(2) - G(1) = -kT\ln[P_2/P_1] \quad (1)$$

where k = 1.38×10^{-23} J/K is the Boltzmann constant, T = 300 K is the simulation temperature, P_2 is the probability for one M molecule to be in state 2, and P_1 is the corresponding probability in state 1. Table 2 also shows ΔG for the transition from unfolded to partially folded states, and from unfolded to folded states. ΔG in water (system 1) has greater values than those in heptane (system 2) and toluene (system 3), confirming the larger energy barrier for the M molecule to transit from unfolded to folded states in water as discussed in Fig. 3.

Table 2. Probabilities that one M molecule is in unfolded, partially folded and folded states, as well as the free energy change estimated from the probabilities.

sys.	solvent	probability (%)			free energy change (kJ/mol)	
		unfolded	partially folded	folded	unfolded to partially folded	unfolded to folded
1	water	91.1	0.9	8.0	11.5	6.1
2	heptane	50.5	15.1	34.4	3.0	1.0
3	toluene	61.4	3.1	35.4	7.4	1.4
4	water	27.1	16.7	56.2	1.2	-1.8
5	heptane	58.8	10.0	31.2	4.4	1.6
6	toluene	61.7	14.3	24.0	3.6	2.4
7	water	78.9	2.6	18.5	8.5	3.6
8	heptane	87.4	6.4	6.1	6.5	6.6
9	toluene	65.3	15.7	19.1	3.6	3.1

The above results show that compared with in heptane and toluene, the M molecule is less flexible in water, has lower probability of being in the folded state and is more likely to be "locked" in the unfolded state due to the energy barrier. Acevedo et al. [37] hypothesized that multi-core PAC molecules would unfold in very good solvents due to solute-solvent affinity. The aromatic nature of toluene usually renders itself as a better solvent than water for PAC molecules. However, the M molecule in our simulations exhibited more likelihood to be unfolded in water than in toluene, which seems contradictory to Acevedo et al.'s hypothesis. One reason is that water can interact with the carboxyl group on the M molecule (evidence in SI Section SI7) which suppresses folding. More importantly, Acevedo et al. considered a PAC solution, not a single PAC molecule as discussed in this section. The folding behaviors of multiple molecules in a solution will be studied next to reveal the relations between folding, flexibility and solubility.

3.2 Folding under homoaggregation

The number of molecules in the largest aggregate for systems with 12 M molecules is shown in Fig. 4a, for the last 10 ns of the simulations. The cut-off minimum distance for two molecules to be considered in an aggregate was set to be 0.35 nm (see SI Section SI8 for detailed explanation on this criterion). A large stable aggregate containing 6 molecules was formed in water, which did not change its size in the last 10 ns. The size of the largest aggregate in heptane fluctuated between 2 and 4 molecules, with an average of 2.6. In toluene, the largest aggregate had up to 3 molecules (average 1.8) and its fluctuation was more frequent. The solubility of M molecules is clearly lowest in water and slightly higher in toluene than in heptane. Snapshots of the largest aggregate in the three solvents are shown in Fig. 4b-d. It should be pointed out that all the 4 molecules in heptane and all the 3 molecules in toluene are shown in the snapshots, although as seen in Fig. 4a some of them detached from the largest aggregates during the simulation. The largest aggregate in water (Fig. 4b) had a spherical shape and the carboxyl tails were located at the surface of the aggregate. In heptane (Fig. 4c), close contact between carboxyl groups was observed in the aggregate, as highlighted by black circles. In toluene (Fig. 4d), the three molecules were considered forming an aggregate based on the minimum distances between them. However, the structure of the aggregate was very loose, and there was no clear evidence for the association of PA cores or carboxyl groups.

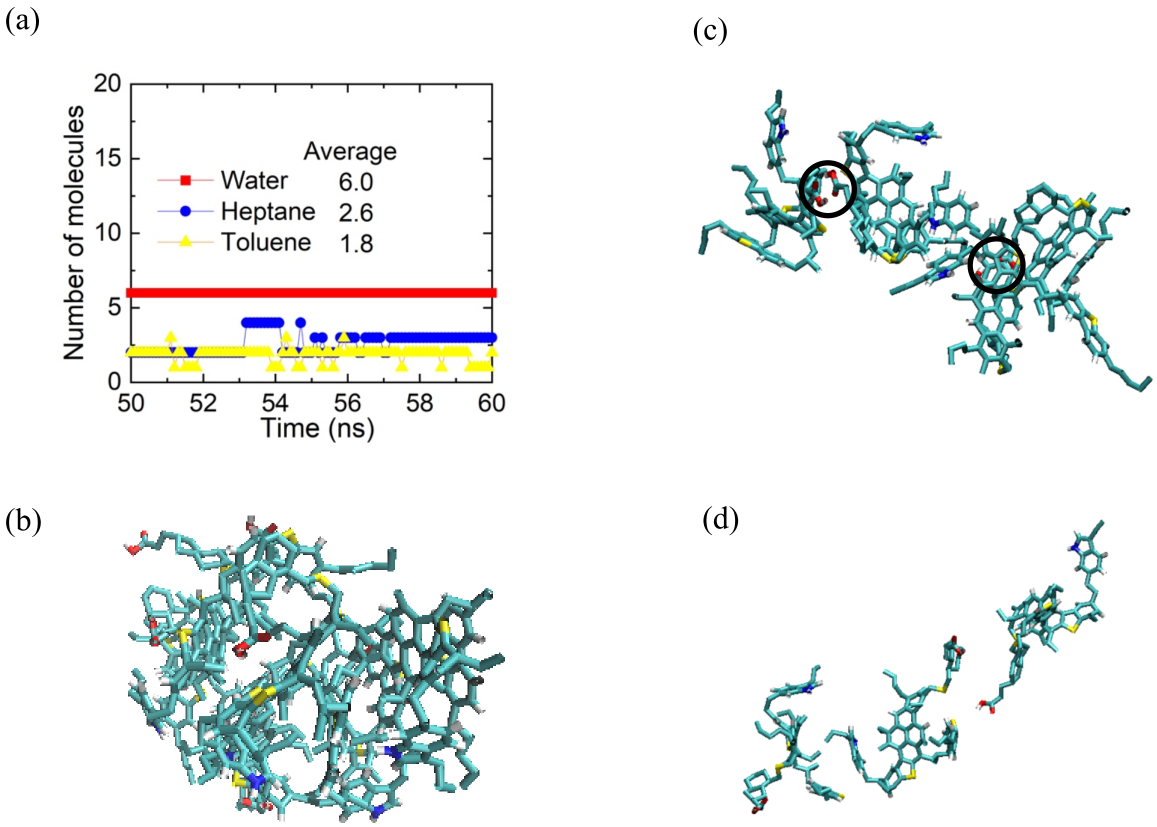

Figure 4. (a) Number of molecules in the largest aggregates over the last 10 ns, for systems with 12 M molecules in water, toluene and heptane. Snapshots of the largest aggregate for systems in (b) water, (d) heptane and (d) toluene.

To investigate the roles of PA cores and carboxyl tails in the aggregation, radial distribution functions (RDFs) between PA cores and carboxyl groups are plotted in Fig. 5a and 5b respectively. RDFs in Fig. 5a were calculated for the COG distance between core1 (see Fig. 1a for its definition) of any two M molecules. Compared with core2 which has 2 aromatic rings, core1 contains 6 rings and is dominant in the π−π interaction between two molecules. To obtain the RDFs in Fig. 5b, each carboxyl group was represented by the COG of its two oxygen atoms. Results for the system in water are shown as red curve in Fig. 5a and 5b. In Fig. 5a, the first and most prominent peak is located at 0.8 nm, which corresponds to a T-shaped stacking where the two cores are nearly perpendicular (see a snapshot in SI Section SI9). In water, there is no evidence of association between carboxyl groups as the curve stays close to zero in Fig. 5b. This is consistent with the fact that the carboxyl groups were located at the outer surface of the sphere-like aggregate (Fig. 4b) with large separation between them. The curve (blue) for heptane in Fig. 5a has a distinct peak at ~1.0 nm. Meanwhile the RDF for the carboxyl groups in Fig. 5b has its first peak located at a much closer distance (~0.28 nm). The result implies that hydrogen bonding between the carboxyl groups made dominant contribution to the aggregation of M molecules in heptane, whereas the interaction between PA cores was limited at close proximity (see a snapshot in SI Section SI9). For toluene (yellow curve in Fig. 5a), there is no obvious peak in the RDF of PA cores. There is a peak in the RDF of the carboxyl groups at a similar location (~ 0.28 nm) to heptane, but the peak value is much smaller. The results suggest that the aggregation of the M molecules in toluene is driven mainly by interaction between carboxyl groups. Interaction between cores is weak, and as such the formed structure is looser compared with those in water and heptane, as seen in Fig. 4d.

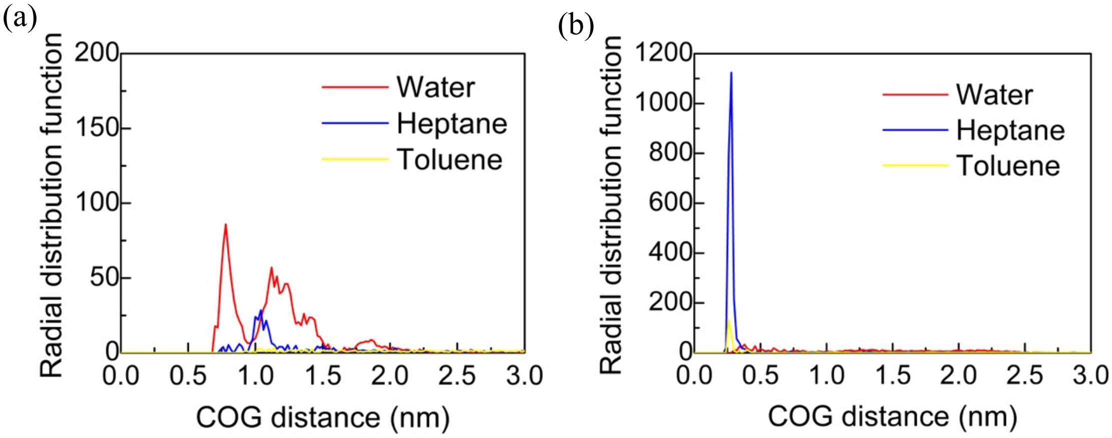

Figure 5. (a) RDFs for the COG distance between core1 (see Fig. 1a for its definition) of any two M molecules; (b) RDFs for the distance between the carboxyl groups of any two M molecules, where each carboxyl group is represented by the COG of the two oxygen atoms. Data are for systems with 12 M molecules and different curves in each subfigure correspond to different solvents (water, toluene and heptane).

Folding behavior of the molecules in the largest aggregates was investigated and shown in Fig. 6. D and θ values were collected along the simulation trajectory for the last 50 ns and plotted against each other. Each subplot corresponds to one molecule. In water, there were 6 molecules in the largest aggregates, labeled as W1 to W6. All 4 molecules in heptane and 3 molecules in toluene shown in Fig. 4c-d were analyzed in Fig. 6. They were labeled as H1 to H4 in heptane, and T1 to T3 in toluene. Among the 6 molecules in water, W2, W3, W4 were mainly in the folded state, and W6 was mainly in the partially folded state. With all of their D values close to 0.55 nm, these molecules had almost zero probability of being in the unfolded state. On the contrary, W5 was exclusively in the unfolded state. Only W1 exhibited both folded and unfolded states throughout the simulation. ΔG for the transition between states is shown in Table S2 (SI Section SI10) for these 6 individual molecules, while the overall ΔG determined from probabilities using data for all

6 molecules is given in Table 2. As described in Fig. 3, there was an energy barrier for a single M molecule in water to switch between folded and unfolded states. With the presence of multiple molecules, it was still difficult for individual M molecules to overcome this barrier (see SI Section SI10 for details), and the transition was lacking for 5 out of the 6 molecules in the largest aggregate. Upon homoaggregation, the internal motions of the molecules within were further restricted, and the molecules were more likely to be "locked" in one of the configuration states. Another interesting observation, from the comparison of Fig. 6 with Fig. 3, is that when a single M molecule was in water the unfolded state was preferred, while in an aggregate the folded state was dominant. This can also be seen in Table 2 where the averaged ΔG from unfolded to folded states is positive for system 1 but negative for system 4. The interactions between the M molecules significantly altered the folding behavior of individual molecules in water. The situation is different in heptane, where the D-θ distributions in Fig. 6 are similar to those shown in Fig. 3 and aggregation did not introduce significant alteration of the folding behaviors. ΔG values in Table 2 further confirm this, showing similar magnitude for systems 2 and 5. Influence of aggregation on folding was also small in toluene, but partial folding which was lacking in Fig. 3 can now be observed for all the molecules in the largest aggregate. Consequently, system 6 has a smaller ΔG from unfolded to partially folded states compared to system 3, as shown in Table 2.

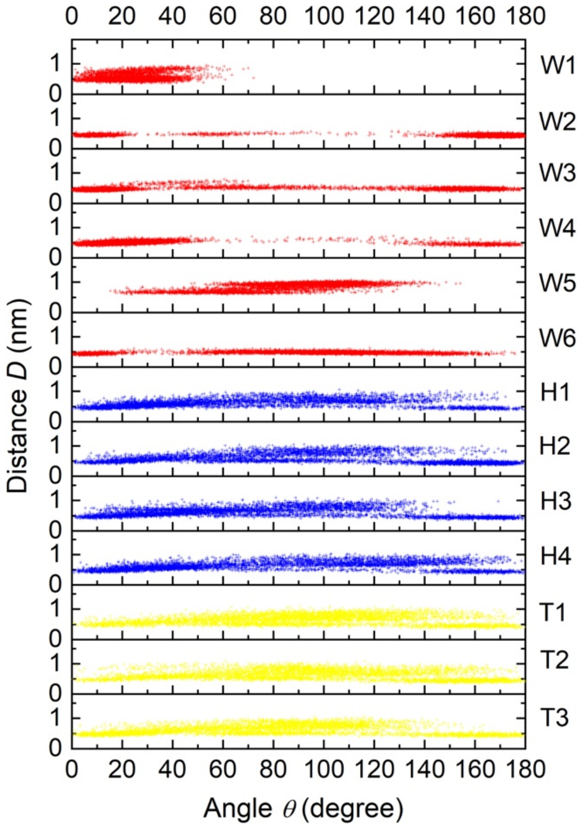

Figure 6. Distance between COGs of core1 and core2 versus angle between the two cores. Data are for individual M molecules in the largest aggregate in water (W1~W6), heptane (H1~H4), and toluene (T1~T3).

A closer look at the interactions between polyaromatic cores and between carboxyl groups (Fig. 5) allows us to further investigate the relation between homoaggregation and folding. In water, the hydrophobic polyaromatic cores repelled water while interacting strongly within the aggregate (Fig. 5a). The tendency to form a compact structure that minimizes core-water interaction and maximizes carboxyl tail-water interaction enhanced folding, changing the dominant configuration from unfolded (for a single molecule) to folded (for molecules in the aggregate). In heptane, the aggregation was achieved mainly through the strong carboxyl-carboxyl association (Fig. 5b).

Core-core interactions were not strong enough to have significant contribution to the aggregation. Such interactions left the molecules in the aggregate with sufficient flexibility to switch between the folded and unfolded configurations. In toluene, the core-core interactions were almost absent and the carboxyl-carboxyl interactions were much weaker than in heptane as seen in Fig. 5. Such weak interactions also allowed the molecules to be flexible and easily switch between folded and unfolded states. On the other hand, the presence of interactions between multiple M molecules, although small, could still shield some interaction between M molecules and toluene so that partially folded configurations could be stabilized. As discussed in Section 3.1, a single M molecule unfolded more in water than in toluene, whereas Acevedo et al. [37] hypothesized that multi-core PAC molecules tended to unfold in good solvent. Here we see that when multiple M molecules were present in water, their folding behavior was significantly altered, with folded configuration being dominant. The molecules in toluene did not experience such a change, and more unfolding is now observed in "good" solvent (toluene) than in "bad" solvent (water), consistent with the hypothesis of Acevedo et al. [37]. Our results not only demonstrate the effects of solvent on the folding of multi-core PACs (see SI Section SI11 for a comparison to folding of multi-core PACs in vacuum), but also highlight the dependence of such effects on the aggregated state of the PAC molecules.

3.3 Folding under heteroaggregation

Since single-core PACs are more prone to aggregation than multi-core PACs, simulations were performed to investigate the effect of adding model S molecules on aggregation, and consequently on the folding of M molecules. Fig. 7 shows the number of molecules in the largest aggregate in systems with a mixture of 6 M molecules and 18 S molecules. In water, all the PAC molecules formed a single large aggregate, which was stable in the last 10 ns of the simulation. There were much more molecules in the largest aggregate in heptane (average 7.1) than in toluene (average 2.5), in agreement with the distinct solubility of single-core PACs in toluene and in heptane [73,74]. Near the end of the simulations, the largest aggregate in heptane contained 1 M and 5 S molecules, while the largest aggregate in toluene contained 1 M and 1 S molecules.

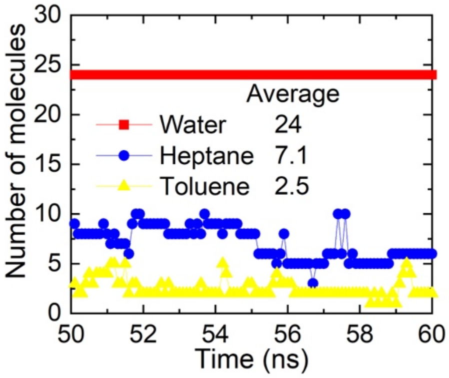

Figure 7. Number of molecules in the largest aggregate of systems containing 6 M molecules and 18 S molecules during the last 10 ns.

D-θ distributions for the M molecules in the largest aggregates are plotted in Fig. 8. In water, W1 to W3 were mainly in the unfolded state (over 89% probability, see SI Section SI10), whereas W4 to W6 had 19.7% to 52.6% of probability to be in the folded states as shown in SI10. The presence of both folded and unfolded states for 3 out of the 6 molecules (W4, W5, W6), as compared to only 1 out of the 6 molecules in Fig. 6, suggests that the M molecules in system 7 were more flexible than those in system 4 which contained only M molecules. Normally, higher flexibility and larger conformation change of individual molecules are detrimental to the stability of aggregation. However, the aggregate in water was large and very stable here due to the presence of S molecules, which dictates the dominating role of S molecules in the heteroaggregation. In fact, the folding characteristics of the M molecules was altered by the aggregation driven by S molecules. Unlike in system 4, the folded state was no longer preferred in system 7, and ΔG from unfolded to folded states was positive as shown in Table 2. The S molecules also influenced the behavior of M molecules in heptane. Firstly, the interaction between M molecules was suppressed and there was only one M molecule in the largest aggregate. Secondly, unlike in system 5 where the M molecules had frequent transitions between folded and unfolded states, the M molecule in the largest aggregate in system 8 was almost exclusively in the unfolded state, which had large ΔG values for the transition out of the unfolded state (Table 2). The interactions between M and S molecules reduced the flexibility of the M molecule, which favored aggregation. Different from that in water and heptane, when S molecules were introduced to toluene, no significant changes were observed for the folding behavior of the M molecules in the aggregates. ΔG from unfolded state to folded or partially folded states were similar between systems 9 and system 6, as shown in Table 2. This can be understood by comparing the degree of homoaggregation (Fig. 4) with that of heteroaggregation (Fig. 7). While the presence of S molecules significantly changed the degree of aggregation in water and in heptane, their influence on the aggregation in toluene was minor. Our findings therefore underline the significant interplay between aggregation and folding.

While previous studies observed self-stacking of multi-core PACs as they aggregate [37,38], the only in-depth investigation on the intramolecular conformational changes of this type of molecules was provided by Wang et al. [39], where a mechanistic connection between aggregation and folding was still absent. Our work, for the first time, compared the folding behaviors of multi-core PACs in isolation vs. in aggregated states, and addressed the effect of aggregation on folding. Homoaggregation and heteroaggregation had different effects, as well changing the type of solvents led to different folding characteristics within the aggregates, which was not studied in previous literatures.

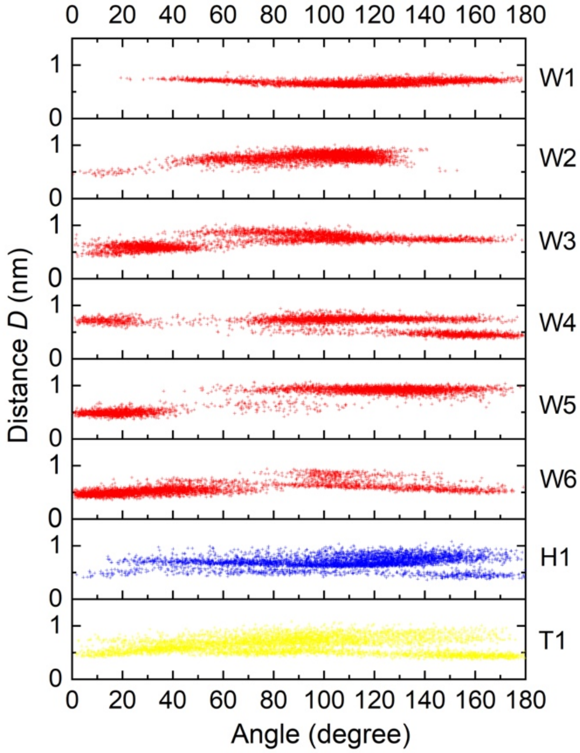

Figure 8. Distance between COGs of core1 and core2 versus angle between the two cores. Data are for individual M molecules in the largest aggregate in systems with a mixture of M and S molecules: in water (W1 to W6), in heptane (H1) and in toluene (T1).

4. Conclusion

This work investigated the folding and aggregation of multi-core polycyclic aromatic compounds (PAC). Solvent was shown to have a strong influence on the structural flexibility of the multi-core PAC molecules. In water, a single dispersed multi-core PAC molecule had small internal flexibility, evidenced by an energy barrier separating folded and unfolded states. The unfolded configuration was dominant and the molecule had a high probability of being “locked” in such a state. When several multi-core PAC molecules were in water and aggregated, the folded state replaced the unfolded state to become dominant, due to the tendency to form a compact structure where the exposure of polyaromatic cores to water was minimized. Introduction of single-core PAC molecules further changed the folding characteristics of multi-core PAC molecules in water due to heteroaggregation. The flexibility of the multi-core PAC molecules was enhanced, and there was more frequent exchange between the folded and unfolded states. In both heptane and toluene, the multi-core PAC molecules were flexible and could easily switch between folded and unfolded states, whether they were dispersed as individual molecules, or in aggregated form. Single-core PAC molecules also altered the folding behavior of multi-core PAC molecules in heptane, making them less flexible, while such effect was not seen in toluene.

Supporting information

Density of M molecules and size for the aggregates (Section SI1); RMSD for a single M molecule (Section SI2); interactions between core1 and core3 (Section SI3); additional discussion on the folded configurations (Section SI4); cut-off distance for folding states (Section SI5); evolution of angle between core1 and core2 (Section SI6); interaction between M molecule and solvents (Section SI7); cut-off distance for aggregation (Section SI8); snapshots of association (Section SI9); free energy change for each M molecule in water (Section SI10); folding of M molecules in vacuum (Section SI11).

Acknowledgement

The authors acknowledge the computing resources and technical support from the Western Canada Research Grid (WestGrid). The authors also gratefully acknowledge the financial support from the

Natural Science and Engineering Research Council of Canada (NSERC) and the Future Energy Systems under the Canada First Research Excellence Fund. We thank Nexen Energy ULC for suggesting the molecular structure of the multi-core PAC, and Dr. Tu Lan for helpful discussions.

Reference

[1] D.J. Hill, M.J. Mio, R.B. Prince, T.S. Hughes, J.S. Moore, A field guide to foldamers, Chem. Rev. 101 (2001) 3893–4011. doi:10.1021/cr990120t.

[2] V.P. Jain, C. Maldarelli, R.S. Tu, Modeling the dynamic folding and surface-activity of a helical peptide adsorbing to a pendant bubble interface, J. Colloid Interface Sci. 331 (2009) 364–370. doi:10.1016/j.jcis.2008.12.016.

[3] A. Steinchen, K. Sefiane, A. Sanfeld, Nano-encapsulation as high pressure devices for folding–unfolding proteins, J. Colloid Interface Sci. 355 (2011) 509–511. doi:10.1016/j.jcis.2010.12.001.

[4] C.M. Dobson, Protein folding and misfolding, Nature. 426 (2003) 884–890. doi:10.1038/nature02261.

[5] W. Zhao, W. Chiuman, J.C.F. Lam, S.A. McManus, W. Chen, Y. Cui, R. Pelton, M.A. Brook, Y. Li, DNA aptamer folding on gold nanoparticles: From colloid chemistry to biosensors, J. Am. Chem. Soc. 130 (2008) 3610–3618. doi:10.1021/ja710241b.

[6] F.M. Menger, L. Shi, S.A.A. Rizvi, Self-assembling systems: Mining a rich vein, J. Colloid Interface Sci. 344 (2010) 241–246. doi:10.1016/j.jcis.2010.01.031.

[7] R. von Wandruszka, Humic acids: Their detergent qualities and potential uses in pollution remediation, Geochem. Trans. 1 (2000) 10–15. doi:10.1039/b001869o.

[8] T. Lan, H. Wang, J. Liao, Y. Yang, Z. Chai, N. Liu, D. Wang, Dynamics of humic acid

and its interaction with uranyl in the presence of hydrophobic surface implicated by molecular dynamics simulations, Environ. Sci. Technol. 50 (2016) 11121–11128. doi:10.1021/acs.est.6b03583.

[9] R. Mezzenga, P. Fischer, The self-assembly, aggregation and phase transitions of food protein systems in one, two and three dimensions, Reports Prog. Phys. 76 (2013). doi:10.1088/0034-4885/76/4/046601.

[10] R. Mezzenga, P. Schurtenberger, A. Burbidge, M. Michel, Understanding foods as soft materials, Nat. Mater. 4 (2005) 729–740. doi:10.1038/nmat1496.

[11] R.J.B.M. Delahaije, P.A. Wierenga, M.L.F. Giuseppin, H. Gruppen, Improved emulsion stability by succinylation of patatin is caused by partial unfolding rather than charge effects, J. Colloid Interface Sci. 430 (2014) 69–77. doi:10.1016/j.jcis.2014.05.019.

[12] E. Sheppard, N. Tcheurekdjian, Monolayer studies. IV. Surface films of emulsion latex particles, J. Colloid Interface Sci. 28 (1968) 481–486. doi:10.1016/0021-9797(68)90080-5.

[13] A. Cornellas, L. Perez, F. Comelles, I. Ribosa, A. Manresa, T.T. Garcia, Self-aggregation and antimicrobial activity of imidazolium and pyridinium based ionic liquids in aqueous solution, J. Colloid Interface Sci. 355 (2011) 164–171. doi:10.1016/j.jcis.2010.11.063.

[14] M.Y. Lin, H.M. Lindsay, D.A. Weitz, R.C. Ball, R. Klein, P. Meakin, Universality in colloid aggregation, Nature. 339 (1989) 360–362. doi:10.1038/339360a0.

[15] H.I. Abdel-Shafy, M.S.M. Mansour, A review on polycyclic aromatic hydrocarbons: Source, environmental impact, effect on human health and remediation, Egypt. J. Pet. 25 (2016) 107–123. doi:10.1016/j.ejpe.2015.03.011.

[16] C. Achten, J.T. Andersson, Overview of polycyclic aromatic compounds (PAC), Polycycl.

Aromat. Compd. 35 (2015) 177–186. doi:10.1080/10406638.2014.994071.

[17] D. Zhang, T.K. Ronson, R. Lavendomme, J.R. Nitschke, Selective separation of polyaromatic hydrocarbons by phase transfer of coordination cages, J. Am. Chem. Soc. 141 (2019) 18949–18953. doi:10.1021/jacs.9b10741.

[18] V. Rajeshkumar, M. Courté, D. Fichou, M.C. Stuparu, Synthesis and properties of large polycyclic aromatic hydrocarbons with planar and non-planar structural motifs, European J. Org. Chem. 2016 (2016) 6010–6014. doi:10.1002/ejoc.201601236.

[19] C. Aumaitre, J.F. Morin, Polycyclic aromatic hydrocarbons as potential building blocks for organic solar cells cyril, Chem. Rec. 19 (2019) 1142–1154. doi:10.1002/tcr.201900016.

[20] K. Müllen, J.P. Rabe, Nanographenes as active components of single-molecule electronics and how a scanning tunneling microscope puts them to work, Acc. Chem. Res. 41 (2008) 511–520. doi:10.1021/ar7001446.

[21] J. Wu, W. Pisula, K. Müllen, Graphenes as potential material for electronics, Chem. Rev. 107 (2007) 718–747. doi:10.1021/cr068010r.

[22] W. Pisula, X. Feng, K. M¨llen, Tuning the columnar organization of discotic polycyclic aromatic hydrocarbons, Adv. Mater. 22 (2010) 3634–3649. doi:10.1002/adma.201000585.

[23] G. Wu, C.Y. Wang, T. Jiao, H. Zhu, F. Huang, H. Li, Controllable self-assembly of macrocycles in water for isolating aromatic hydrocarbon isomers, J. Am. Chem. Soc. 140 (2018) 5955–5961. doi:10.1021/jacs.8b01651.

[24] F.S. Kim, G. Ren, S.A. Jenekhe, One-dimensional nanostructures of π-conjugated molecular systems: Assembly, properties, and applications from photovoltaics, sensors, and nanophotonics to nanoelectronics, Chem. Mater. 23 (2011) 682–732.

doi:10.1021/cm102772x.

[25] C. Alvariño, E. Pía, M.D. García, V. Blanco, A. Fernández, C. Peinador, J.M. Quintela, Dimensional matching of polycyclic aromatics with rectangular metallacycles: Insertion modes determined by [C-Hπ] interactions, Chem. - A Eur. J. 19 (2013) 15329–15335. doi:10.1002/chem.201302165.

[26] Z. Zhang, D.S. Kim, C.Y. Lin, H. Zhang, A.D. Lammer, V.M. Lynch, I. Popov, O.S. Miljanić, E. V Anslyn, J.L. Sessler, Expanded porphyrin-anion supramolecular assemblies: environmentally responsive sensors for organic solvents and anions, J. Am. Chem. Soc. 137 (2015) 7769–7774. doi:10.1021/jacs.5b03131.

[27] S. Origuchi, M. Kishimoto, M. Yoshizawa, S. Yoshimoto, A supramolecular approach to the preparation of nanographene adlayers using water-soluble molecular capsules, Angew. Chemie - Int. Ed. 57 (2018) 15481–15485. doi:10.1002/anie.201809258.

[28] A. Narita, X.-Y. Wang, X. Feng, K. Mü, New advances in nanographene chemistry, Chem. Soc. Rev. 44 (2015) 6616. doi:10.1039/c5cs00183h.

[29] D. Wasserfallen, M. Kastler, W. Pisula, W.A. Hofer, Y. Fogel, Z. Wang, K. Müllen, Suppressing aggregation in a large polycyclic aromatic hydrocarbon, J. Am. Chem. Soc. 128 (2006) 1334–1339. doi:10.1021/ja056782j.

[30] F.S. Kim, G. Ren, S.A. Jenekhe, One-dimensional nanostructures of π-conjugated molecular systems: Assembly, properties, and applications from photovoltaics, sensors, and nanophotonics to nanoelectronics, Chem. Mater. 23 (2011) 682–732. doi:10.1021/cm102772x.

[31] B.D. Adamson, S.A. Skeen, M. Ahmed, N. Hansen, Detection of aliphatically bridged multi-core polycyclic aromatic hydrocarbons in sooting flames with atmospheric-sampling

high-resolution tandem mass spectrometry, J. Phys. Chem. A. 122 (2018) 9338–9349. doi:10.1021/acs.jpca.8b08947.

[32] J.M. Mativetsky, M. Kastler, R.C. Savage, D. Gentilini, M. Palma, W. Pisula, K. Müllen, P. Samorì, Self-assembly of a donor-acceptor dyad across multiple length scales: functional architectures for organic electronics, Adv. Funct. Mater. 19 (2009) 2486–2494. doi:10.1002/adfm.200900366.

[33] K. Hąc-Wydro, K. Połeć, M. Broniatowski, The impact of selected polycyclic aromatic hydrocarbons (PAHs) on the morphology, stability and relaxation of ternary lipid monolayers imitating soil bacteria membrane, J. Mol. Liq. 276 (2019) 409–416. doi:10.1016/j.molliq.2018.12.020.

[34] A. Tirjoo, B. Bayati, H. Rezaei, M. Rahmati, Molecular dynamics simulation of the effect of ions in water on the asphaltene aggregation, J. Mol. Liq. 277 (2019) 40–48. doi:10.1016/j.molliq.2018.12.067.

[35] J.A. González, M. Zawadzki, U. Domanska, Thermodynamics of mixtures containing polycyclic aromatic hydrocarbons, J. Mol. Liq. 143 (2008) 134–140. doi:10.1016/j.molliq.2008.07.005.

[36] H. Jin, W. Ding, B. Chen, B. Bai, Q. Zhao, C. Cao, A molecular dynamics simulation investigation on the solubility of polycyclic aromatic hydrocarbons in supercritical water, J. Mol. Liq. 301 (2020). doi:10.1016/j.molliq.2020.112464.

[37] S. Acevedo, A. Castro, E. Vásquez, F. Marcano, M.A. Ranaudo, Investigation of physical chemistry properties of asphaltenes using solubility parameters of asphaltenes and their fractions A1 and A2, Energy & Fuels. 24 (2010) 5921–5933. doi:10.1021/ef1005786.

[38] T. Kuznicki, J.H. Masliyah, S. Bhattacharjee, Molecular dynamics study of model

molecules resembling asphaltene-like structures in aqueous organic solvent systems, Energy & Fuels. 22 (2008) 2379–2389. doi:10.1021/ef800057n.

[39] J. Wang, M. Gayatri, A.L. Ferguson, Coarse-grained molecular simulation and nonlinear manifold learning of archipelago asphaltene aggregation and folding, J. Phys. Chem. B. 122 (2018) 6627–6647. doi:10.1021/acs.jpcb.8b01634.

[40] M.J. Frisch, G.W. Trucks, H.B. Schlegel, G.E. Scuseria, M.A. Robb, J.R. Cheeseman, G. Scalmani, V. Barone, G.A. Petersson, H. Nakatsuji, X. Li, M. Caricato, A. V Marenich, J. Bloino, B.G. Janesko, R. Gomperts, B. Mennucci, H.P. Hratchian, J. V Ortiz, A.F. Izmaylov, J.L. Sonnenberg, D. Williams-Young, F. Ding, F. Lipparini, F. Egidi, J. Goings, B. Peng, A. Petrone, T. Henderson, D. Ranasinghe, V.G. Zakrzewski, J. Gao, N. Rega, G. Zheng, W. Liang, M. Hada, M. Ehara, K. Toyota, R. Fukuda, J. Hasegawa, M. Ishida, T. Nakajima, Y. Honda, O. Kitao, H. Nakai, T. Vreven, K. Throssell, J.A. Montgomery Jr., J.E. Peralta, F. Ogliaro, M.J. Bearpark, J.J. Heyd, E.N. Brothers, K.N. Kudin, V.N. Staroverov, T.A. Keith, R. Kobayashi, J. Normand, K. Raghavachari, A.P. Rendell, J.C. Burant, S.S. Iyengar, J. Tomasi, M. Cossi, J.M. Millam, M. Klene, C. Adamo, R. Cammi, J.W. Ochterski, R.L. Martin, K. Morokuma, O. Farkas, J.B. Foresman, D.J. Fox, Gaussian 16, revision C.01, (2016).

[41] A.B. Andrews, A. McClelland, O. Korkeila, A. Demidov, A. Krummel, O.C. Mullins, Z. Chen, Molecular orientation of asphaltenes and PAH model compounds in langmuir-blodgett films using sum frequency generation spectroscopy, Langmuir. 27 (2011) 6049–6058. doi:10.1021/la200466b.

[42] A.K. Malde, L. Zuo, M. Breeze, M. Stroet, D. Poger, P.C. Nair, C. Oostenbrink, A.E. Mark, An Automated force field Topology Builder (ATB) and repository: Version 1.0, J.

Chem. Theory Comput. 7 (2011) 4026–4037. doi:10.1021/ct200196m.

[43] G. Heerdt, I. Tranca, A.J. Markvoort, B.M. Szyja, N.H. Morgon, E.J.M. Hensen, Photoisomerization induced scission of rod-like micelles unravelled with multiscale modeling, J. Colloid Interface Sci. 510 (2018) 357–367. doi:10.1016/j.jcis.2017.09.036.

[44] J.A. Lemkul, D.R. Bevan, Assessing the stability of Alzheimer's amyloid protofibrils using molecular dynamics, J. Phys. Chem. B. 114 (2010) 1652–1660. doi:10.1021/jp9110794.

[45] J.A. Lemkul, W.J. Allen, D.R. Bevan, Practical considerations for building GROMOS-compatible small-molecule topologies, J. Chem. Inf. Model. 50 (2010) 2221–2235. doi:10.1021/ci100335w.

[46] D. Van Der Spoel, E. Lindahl, B. Hess, G. Groenhof, A.E. Mark, H.J.C. Berendsen, GROMACS: Fast, flexible, and free, J. Comput. Chem. 26 (2005) 1701–1718. doi:10.1002/jcc.20291.

[47] J. Liu, X. Li, W. Jia, Z. Li, Y. Zhao, S. Ren, Demulsification of crude oil-in-water emulsions driven by graphene oxide nanosheets, Energy & Fuels. 29 (2015) 4644–4653. doi:10.1021/acs.energyfuels.5b00966.

[48] C.M. Breneman, K.B. Wiberg, Determining atom-centered monopoles from molecular electrostatic potentials. The need for high sampling density in formamide conformational analysis, J. Comput. Chem. 11 (1990) 361–373. doi:10.1002/jcc.540110311.

[49] R.J. Ferreira, M.J.U. Ferreira, D.J.V.A. Dos Santos, Insights on P-glycoproteins efflux mechanism obtained by molecular dynamics simulations, J. Chem. Theory Comput. 8 (2012) 1853–1864. doi:10.1021/ct300083m.

[50] N.E. Jackson, K.L. Kohlstedt, B.M. Savoie, M. Olvera De La Cruz, G.C. Schatz, L.X.

Chen, M.A. Ratner, Conformational order in aggregates of conjugated polymers, J. Am. Chem. Soc. 137 (2015) 6254–6262. doi:10.1021/jacs.5b00493.

[51] P.R. Arantes, M.D. Polêto, E.B.O. John, C. Pedebos, B.I. Grisci, M. Dorn, H. Verli, Development of GROMOS-compatible parameter set for simulations of chalcones and flavonoids, J. Phys. Chem. B. 123 (2019) 994–1008. doi:10.1021/acs.jpcb.8b10139.

[52] C. Jian, T. Tang, S. Bhattacharjee, Probing the effect of side-chain length on the aggregation of a model asphaltene using molecular dynamics simulations, in: Energy & Fuels, 2013: pp. 2057–2067. doi:10.1021/ef400097h.

[53] J. Dufour, J.A. Calles, J. Marugán, R. Giménez-Aguirre, J.L. Peña, D. Merino-García, Influence of hydrocarbon distribution in crude oil and residues on asphaltene stability, Energy & Fuels. 24 (2010) 2281–2286. doi:10.1021/ef900934t.

[54] J.M. Sheremata, M.R. Gray, H.D. Dettman, W.C. McCaffrey, Quantitative molecular representation and sequential optimization of Athabasca asphaltenes, Energy & Fuels. 18 (2004) 1377–1384. doi:10.1021/ef049936+.

[55] X. Zhu, G. Wu, D. Chen, Molecular dynamics simulation of cyclodextrin aggregation and extraction of Anthracene from non-aqueous liquid phase, J. Hazard. Mater. 320 (2016) 169–175. doi:10.1016/j.jhazmat.2016.08.015.

[56] A. Srivastava, K. Ismail, Solubilization of polycyclic aromatic hydrocarbons in aqueous sodium dioctylsulfosuccinate solutions, J. Mol. Liq. 195 (2014) 105–109. doi:10.1016/j.molliq.2014.02.007.

[57] C. Wu, A. De Visscher, I.D. Gates, Molecular interactions between 1-butyl-3-methylimidazolium tetrafluoroborate and model naphthenic acids: A DFT study, J. Mol. Liq. 243 (2017) 462–471. doi:10.1016/j.molliq.2017.08.061.

[58] M. Maes, M. Trekels, M. Boulhout, S. Schouteden, F. Vermoortele, L. Alaerts, D. Heurtaux, Y.K. Seo, Y.K. Hwang, J.S. Chang, I. Beurroies, R. Denoyel, K. Temst, A. Vantomme, P. Horcajada, C. Serre, D.E. De Vos, Selective removal of N-heterocyclic aromatic contaminants from fuels by lewis acidic metal-organic frameworks, Angew. Chemie - Int. Ed. 50 (2011) 4210–4214. doi:10.1002/anie.201100050.

[59] H. Sharghi, R. Khalifeh, A.R. Salimi Beni, Synthesis of new lariat ethers containing polycyclic phenols and heterocyclic aromatic compound on graphite surface via mannich reaction, J. Iran. Chem. Soc. 7 (2010) 275–288. doi:10.1007/BF03245889.

[60] J. Taheri-Shakib, N. Saadati, A. Esfandiarian, S.A. Hosseini, M. Rajabi-Kochi, Characterizing the wax-asphaltene interaction and surface morphology using analytical spectroscopy and microscopy techniques, J. Mol. Liq. 302 (2020). doi:10.1016/j.molliq.2020.112506.

[61] C. Jian, T. Tang, One-dimensional self-assembly of polyaromatic compounds revealed by molecular dynamics simulations, J. Phys. Chem. B. 118 (2014) 12772–12780. doi:10.1021/jp506381z.

[62] R.N. Nagrimanov, A.A. Samatov, B.N. Solomonov, Additive scheme of solvation enthalpy for linear, cyclic and branched-chain aliphatic compounds at 298.15 K, J. Mol. Liq. 292 (2019). doi:10.1016/j.molliq.2019.111365.

[63] R. Dutta Majumdar, T. Montina, O.C. Mullins, M. Gerken, P. Hazendonk, Insights into asphaltene aggregate structure using ultrafast MAS solid-state1H NMR spectroscopy, Fuel. 193 (2017) 359–368. doi:10.1016/j.fuel.2016.12.082.

[64] J. Eyssautier, P. Levitz, D. Espinat, J. Jestin, J. Gummel, I. Grillo, L. Barré, Insight into asphaltene nanoaggregate structure inferred by small angle neutron and X-ray scattering,

J. Phys. Chem. B. 115 (2011) 6827–6837. doi:10.1021/jp111468d.

[65] T. Lan, H. Zeng, T. Tang, Understanding adsorption of Violanthrone-79 as a model asphaltene compound on quartz surface using molecular dynamics simulations, J. Phys. Chem. C. 122 (2018) 28787–28796. doi:10.1021/acs.jpcc.8b09712.

[66] T. Lan, H. Zeng, T. Tang, Molecular dynamics study on the mechanism of graphene oxide to destabilize oil/water emulsion, J. Phys. Chem. C. 123 (2019) 22989–22999. doi:10.1021/acs.jpcc.9b05906.

[67] B. Hess, P-LINCS: A parallel linear constraint solver for molecular simulation, J. Chem. Theory Comput. 4 (2008) 116–122. doi:10.1021/ct700200b.

[68] E. Lindahl, B. Hess, D. van der Spoel, GROMACS 3.0: A package for molecular simulation and trajectory analysis, J. Mol. Model. 7 (2001) 306–317. doi:10.1007/S008940100045.

[69] H.J.C. Berendsen, D. van der Spoel, R. van Drunen, GROMACS: A message-passing parallel molecular dynamics implementation, Comput. Phys. Commun. 91 (1995) 43–56. doi:10.1016/0010-4655(95)00042-E.

[70] C. Oostenbrink, T.A. Soares, N.F.A. Van Der Vegt, W.F. Van Gunsteren, Validation of the 53A6 GROMOS force field, Eur. Biophys. J. 34 (2005) 273–284. doi:10.1007/s00249-004-0448-6.

[71] U. Essmann, L. Perera, M.L. Berkowitz, T. Darden, H. Lee, L.G. Pedersen, A smooth particle mesh Ewald method, J. Chem. Phys. 103 (1995) 8577–8593. doi:10.1063/1.470117.

[72] W.F. Van Gunsteren, X. Daura, A.E. Mark, Computation of free energy, Helv. Chim. Acta. 85 (2002) 3113–3129. doi:10.1002/1522-2675(200210)85:10<3113::AID-

HLCA3113>3.0.CO;2-0.

[73] C. Jian, T. Tang, Molecular dynamics simulations reveal inhomogeneity-enhanced stacking of violanthrone-78-based polyaromatic compounds in n-heptane-toluene mixtures, J. Phys. Chem. B. 119 (2015) 8660–8668. doi:10.1021/acs.jpcb.5b04481.

[74] Y. Aray, R. Hernández-Bravo, J.G. Parra, J. Rodríguez, D.S. Coll, Exploring the structure-solubility relationship of asphaltene models in toluene, heptane, and amphiphiles using a molecular dynamic atomistic methodology, J. Phys. Chem. A. 115 (2011) 11495–11507. doi:10.1021/jp204319n.